Exploring miniaturized HVOF systems for the deposition of Ti-6Al-4V

Oberste-Berghaus, J.; Aghasibeig, M.; Burgess, A.; Khamsepour, P.; Moreau, C.; Dolatabadi, A.

Publisher's version / Version de l'éditeur:
https://doi.org/10.1007/s11666-023-01531-3
Journal of Thermal Spray Technology, 32, 2-3, pp. 760-772, 2023-01-25

J Therm Spray Tech (2023) 32:760–772
https://doi.org/10.1007/s11666-023-01531-3

PEER REVIEWED

Exploring Miniaturized HVOF Systems for the Deposition of Ti-6Al-4V

J. Oberste-Berghaus[1] · M. Aghasibeig[1] · A. Burgess[2] · P. Khamsepour[3] · C. Moreau[3] · A. Dolatabadi[4]

Submitted: 22 August 2022 / in revised form: 13 December 2022 / Accepted: 21 December 2022 / Published online: 25 January 2023

Abstract The exceptional properties of Ti-6Al-4V of high strength, lightweight, corrosion resistance and machinability make it one of the most widely used alloys in in the aerospace industry. Significant efforts are underway to establish powder bed additive manufacturing technologies for Ti-6Al-4V. There are also increasing attempts to use thermal and cold spray to build near-net-shaped parts with buildup rates orders of magnitude higher than powder bed. Thermal spraying, such as HVOF, can oxidize and degrade the alloy due to the high processing temperature. Lowering the flame temperature through inert gas addition in full-size HVOF systems is a possible approach to retain solid-state deposition of the feedstock particles, thereby limiting oxidation and detrimental α-case formation, while providing sufficient heat input for particle softening and plastic deformation at impact. Novel miniaturized HVOF systems, with spray jets of only a few millimeters in width, may further offer the possibility to improve the spatial resolution of the buildup for near-net shape forming. The process parameter range for solid-state deposition of Ti-6A-4V using the liquid-fuelled TAFA Model 825 JP*id* and the novel hydrogen-fuelled Spraywerx ID-NOVA MK-6 with the addition of nitrogen is shown. Buildups at over 80% deposition efficiency generally yield as-sprayed porosities below 3% and hardness above 200 HV_{100gf}. Attainable microstructures and oxygen content as a function of spray parameters are delineated. Recrystallization and beta-annealing of selected samples lower the residual porosity and can create equiaxed α and intergranular ß-phases. Ultimate tensile strengths of up to 1100 MPa were attained; however, the residual oxygen content of above 0.7% was found to limit β-phase formation, which contributes to a limited elongation to failure.

Keywords miniature HVOF · near-net shape forming · tensile strength · Ti-6Al-4V · warm spraying

This article is an invited paper selected from presentations at the 2022 International Thermal Spray Conference, held May 4–6, 2022 in Vienna, Austria, and has been expanded from the original presentation. The issue was organized by André McDonald, University of Alberta (Lead Editor); Yuk-Chiu Lau, General Electric Power; Fardad Azarmi, North Dakota State University; Filofteia-Laura Toma, Fraunhofer Institute for Material and Beam Technology; Heli Koivuluoto, Tampere University; Jan Cizek, Institute of Plasma Physics, Czech Academy of Sciences; Emine Bakan, Forschungszentrum Jülich GmbH; Šárka Houdková, University of West Bohemia; and Hua Li, Ningbo Institute of Materials Technology and Engineering, CAS.

✉ J. Oberste-Berghaus
Jorg.Oberste-Berghaus@cnrc-nrc.gc.ca

[1] National Research Council Canada, Boucherville, Québec, Canada

[2] Spraywerx Technologies Inc., North Vancouver, BC, Canada

[3] Department of Mechanical, Industrial and Aerospace Engineering, Concordia University, Montreal, Québec, Canada

[4] Department of Mechanical and Industrial Engineering, University of Toronto, Toronto, ON, Canada

Introduction

Application of titanium alloys in the aerospace industry is driven by their superior properties such as high strength, fatigue resistance and creep resistance at low-to-moderate temperatures in combination with low density and low modulus (high flexibility). Because of difficulties in casting and welding of titanium alloys due to the high affinity to oxygen and the high solid solubility of oxygen (about 14.5%) (Ref 1), there is a demand for direct fabrication of

Table 1 TAFA Model 825 JP*id* Parameters

Kerosene flow rates	7, 8, 8.5 and 9 L per hour (lph)
Oxygen flow rates	300 and 620 standard liters per minute (slpm)
Nitrogen flow rates	360 and 575 slpm
Combustion pressures	130-150 psi
Standoff distance	25.4, 38.1 and 50.8 mm
Gun travers speed	1500 mm/sec
Pitch	1.3 mm
Powder feed rate	20 g/min

Table 2 Spraywerx ID-Nova MK-6 Parameters

Hydrogen flow rate	250-300 slpm
Oxygen flow rates	125-150 slpm
Nitrogen flow rates	250 slpm
Combustion pressures	200-250 psi
Standoff distance	40 mm
Gun travers speed	1500 mm/sec
Pitch	1.3 mm
Powder feed rate	10 g/min

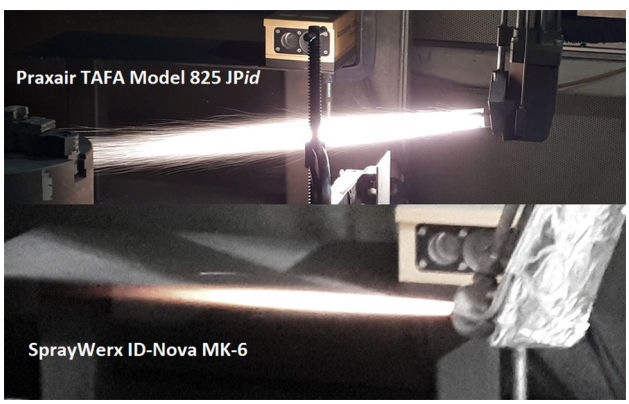

Fig. 1 Photographs of the TAFA Model 825 JP*id* and ID-Nova MK-6 during Ti-6A-4V spraying

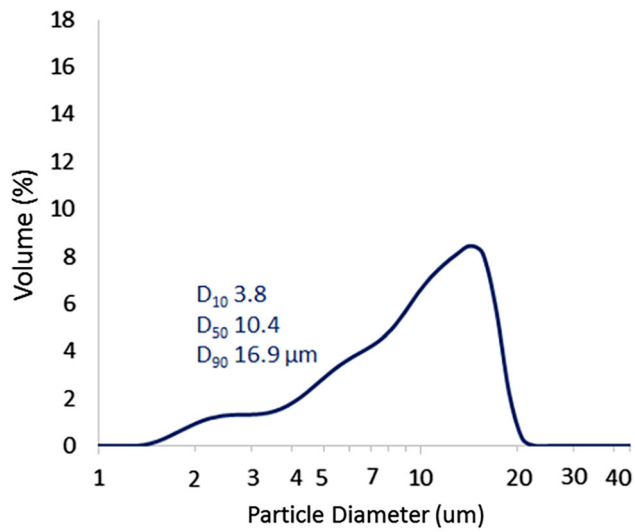

Fig. 2 Particle size distribution of Ti-6Al-4V grade 5

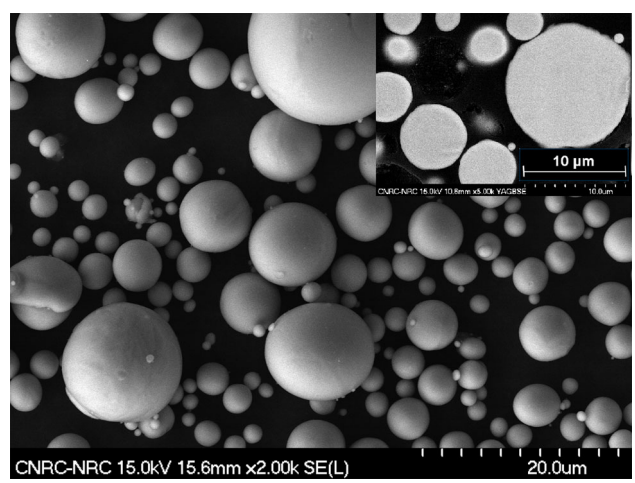

Fig. 3 SEM micrograph of Ti-6Al-4V feedstock at 2kX mag (insert—backscattered image of cross section of powder at 5kX mag)

metal parts in near-net shapes (NNS), which can produce complex components with minimal waste of material (Ref 2). Various processing techniques like plasma spraying, selective laser melting and electron beam melting have previously been used to deposit Ti and its alloys as coatings (Ref 3–5) or near-net-shaped parts. These techniques involve high working temperatures resulting in phase transformations, tensile residual stresses and high-temperature oxidation. One of the techniques that have been explored is low-pressure plasma spray (LPPS). It suppresses the oxidation of the feedstock powder through operation in an inert atmosphere under low-pressure conditions (Ref 6). The LPPS equipment costs are rather high, and this investment can only be justified in exceptional cases. An alternative approach is to use cold spray technology to deposit the material well below the melting point and attaining deposition through plastic deformation of impacting particles, minimizing or eliminating the deleterious effects of high-temperature oxidation, phase transformations and/or tensile residual stresses (Ref 7–9). Furthermore, the cold spray process is highly conducive in building a high-resolution, near-net-shaped feature not only

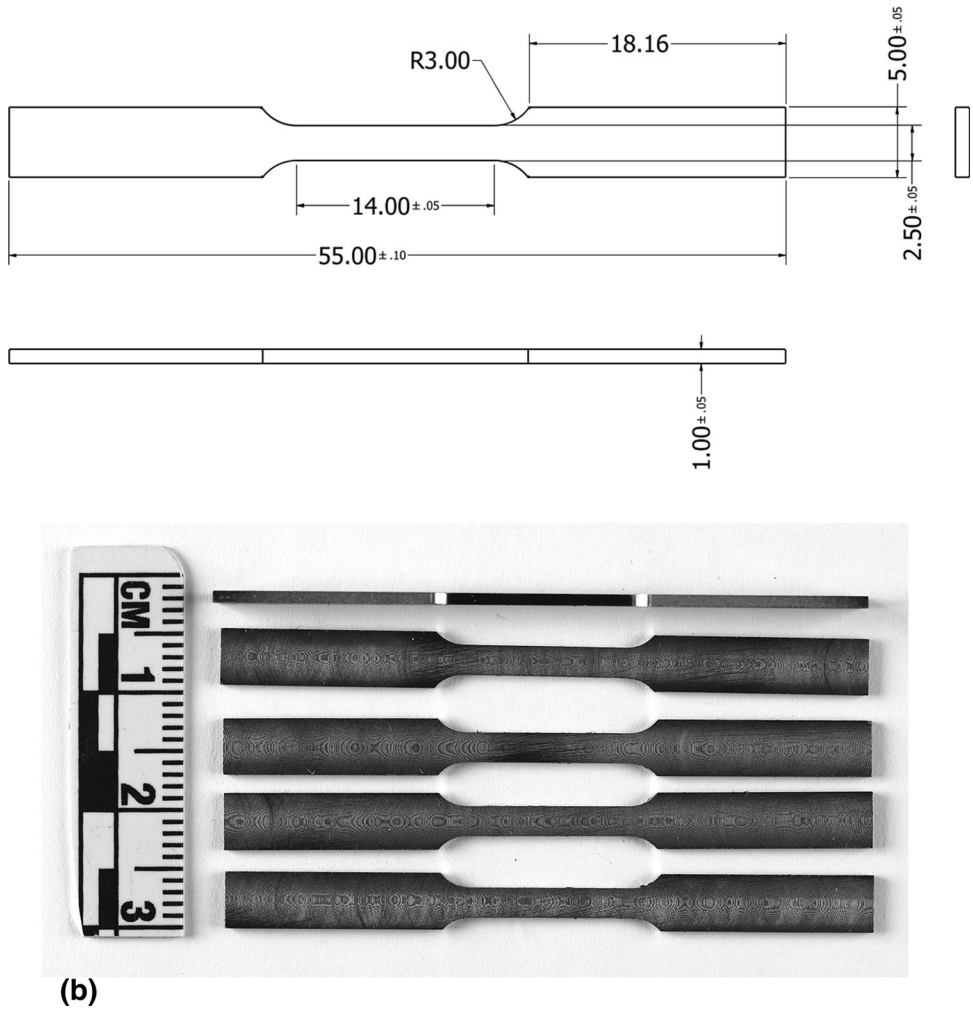

Fig. 4 Tensile specimen dimensions (mm) based on ASTM E8/E8M-22 –sub-size specimen

by virtue of its spatially restricted spray jet of a few millimeters, but also because its sensitivity to the angle of particle impact, which can be exploited to control the deposit shape. In spite of its promise, cold spray deposition of high-yield-strength materials like Ti6Al4V remains very challenging (Ref 10–13). Prior works illustrate that the high yield strength of Ti6Al4V makes it extremely difficult to cold spray and the resultant coatings had high porosity (Ref 11, 12, 14–16), mainly because of the high critical velocity required to form bonding between deposited particles. Vo et al., Khun et al. and Bhattiprolu et al. deposited Ti6Al4V coatings using Nitrogen (N_2) and Helium (He) as propellant gas (Ref 11, 12, 17–20). The shortage and high cost of helium necessitates a gas recycling facility, a large initial investment, rendering the use of He non-viable. However, using the more economical N_2, fully dense coatings with high tensile strength could not be yet be obtained, even though the most recent CS equipment operates with a gas pressure of 4 MPa and a temperature close to 1000 °C. Alternatively, the effects of powder morphology on the cold-sprayed deposit were studied by McDonald et al. (Ref 18) and Munagala et al. (Ref 21), and the porosity of the as-sprayed coating was significantly reduced by employing powder with irregular morphology instead of the more standard sphere-shaped particles. Although improving the density, the deposits properties were still far below the desired bulk properties in terms of ultimate tensile strength and elongation of Ti-6Al-4V wrought material ($\sigma UTS_{bulk} > 828$ MPa). A recent approach is proposed by Molak et al. (Ref 17, 22), modifying a high-velocity oxy-fuel (HVOF) spraying process to produce Ti-6Al-4V coatings in a process referred to as warm spraying (WS). In this process, the temperature of a supersonic gas flow generated by combustion of a fuel and oxygen is controlled by diluting the combustion flame with an inert gas such as nitrogen. Such approach raises the processing temperature only slightly above the cold spray process to attain enhanced material softening, while achieving similar or better particle deformation through gas velocities comparable to the cold spray process. Fine tuning of the spray process parameter and post-heat treatment, in particular through beta- and recrystallization annealing,

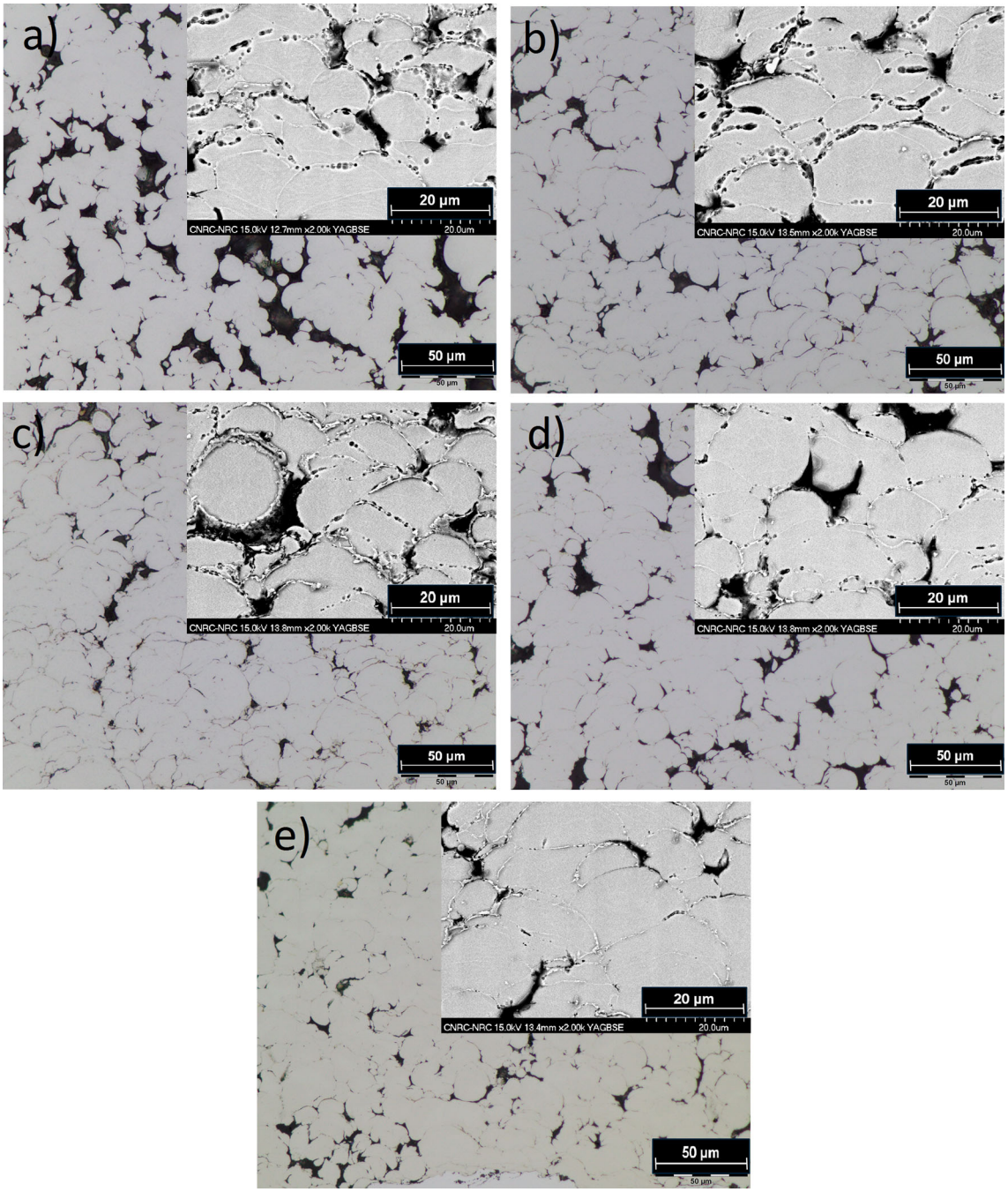

Fig. 5 Cross-sectional optical images (500 ×) of Ti-6Al-4V coatings fabricated at 50.8 mm standoff distance with high oxygen (620 slpm)/low nitrogen (360 slpm) at **a** 7 lph kerosene, **b** 8 lph kerosene, **c** 8.5 lph kerosene and low oxygen (300 slpm)/high nitrogen (575 slpm) at **d** 8 lph kerosene, **e** 9 lph kerosene (inserts: SEM micrographs of etched cross section at 2000 × original magnification, showing different degrees of particle boundary attack by the etchant)

Ti-6Al-4V deposits approaching LPPS deposit properties in terms of elongation to failure and even close to bulk Ti-6Al-4V in terms of Ultimate tensile strength σUTS > 800 MPa were demonstrated. The key limitation of the current warm spray approach, although highly scalable to near-net-shape forming of aerospace parts and component overhaul by virtue of its operation in the open atmosphere, is the wide spray jet and lack of spatial resolution of the deposit. To allow high-resolution near-net-shape forming as relevant for aerospace components, spray jets in the order of a few millimeters would be far more suitable. Novel initiatives to design miniaturized spray systems could be adopted to address this gap. This study explores miniaturized inner diameter TAFA Model 825 JP*id* and the

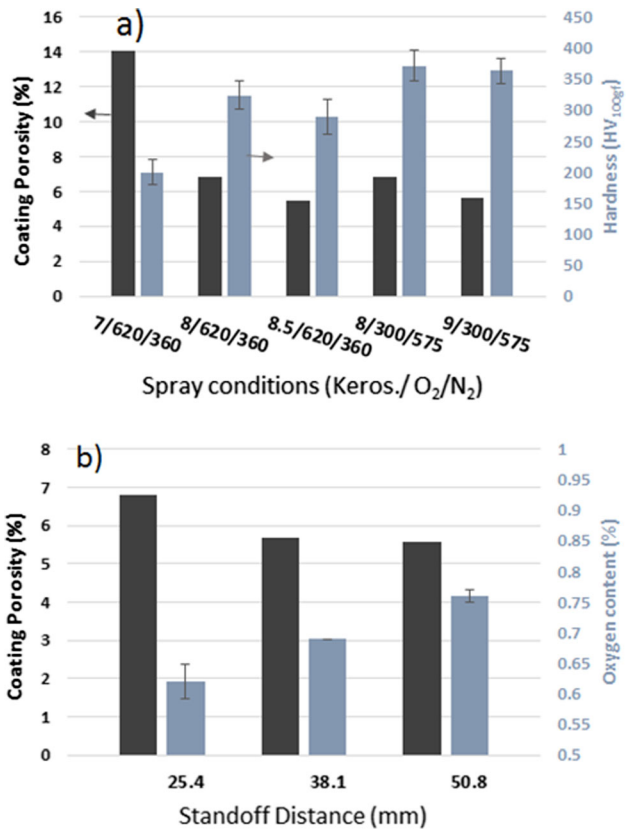

Fig. 6 Evolution of **a** coating porosity and hardness for with increasing kerosene and nitrogen flow at 50.8 mm standoff distance and **b** coating porosity and oxygen content as a function of standoff distance at highest kerosene and nitrogen flow at 9 lph Keros./ 300 slpm O_2/575 slpm N_2

Fig. 7 Photograph of Ti-6Al-4V buildup of approximately 5 mm thickness on 114-mm-diameter steel mandrel

Spraywerx ID-Nova MK-6 HVOF systems, which were modified to allow nitrogen addition to create a miniaturized warm spray apparatus. The goals are to tune the Ti-6Al-4V powder softening and acceleration for solid-state deposition of dense coatings, while maintaining a high-resolution jet and minimizing in-flight oxidation. Alternatively, high-velocity air–fuel system HVAF, as miniaturized in the Uniquecoat i7 for example, is based on the principle of using air instead of oxygen as the oxidant, thereby creating a combustion environment containing fuel, oxygen and nitrogen, similar to warm spraying. HVAF solid-state deposition of Ti6Al4V is detailed by P. Khamsepour et al. (Ref 23).

Materials and Processes

Two distinctly different miniaturized HVOF systems were employed in this study: the TAFA Model 825 JP*id* (Praxair Surface Technologies Inc.), a kerosene-fuelled HP/HVOF gun with power levels in the range of 140 kW, originally designed for tight confines of "Francise" turbine vanes or inner diameters as small as 8″ /204 mm, and the smaller ID-Nova MK-6 (Spraywerx Technologies Inc, Vancouver), a hydrogen-fuelled HVOF gun designed for inner diameters as small as 4″/102 mm with powder levels in the range of 60-80 kW. For both systems, nitrogen was added to the combustion in an attempt to reduce the combustion temperature and increase the gas velocity avoiding particle melting and fostering a solid-state deposition of Ti-6Al-4V. Further, these systems feature a narrow particle jet of less than 8 or less than 6 mm width, conducive to a finer special resolution than attainable in conventional HVOF systems for the creation of near-net shapes. Key parameter ranges are summarized in Table 1 and 2 for the TAFA Model 825 JP*id* and ID-Nova MK-6, respectively. Limiting the heat input to promote solid-state deposition, the 825 JP*id* kerosene system was operated only up to a net power of 70 kW. The effects of power input, nitrogen addition and standoff distance on the resulting coating characteristics are investigated. The ID-Nova MK-6 was operated at net power levels not exceeding 52 kW. The effect of power input on the coating characteristics was studied. Figure 1 shows photographs of the TAFA Model 825 JP*id* and ID-Nova MK-6 during Ti-6A-4 V spraying, respectively, featuring highly luminous spray jets. The brightness of the jet is attributed to in-flight combustion of some portion of the titanium powder fines.

All coatings were produced on grit basted (60 grit alumina) mild steel coupons or tube substrates. Forced air and nitrogen cooling was used to limit the surface temperature during deposition to below 200 °C.

Spherical Ti-6Al-4V grade 5 powders from AP&C (Boisbriand, Canada) were used in this study. Particle sizes, as measured with a Coulter LS (Hialeah, FL) particle size analyzer, show a wide distribution around the D_{50} of 10.4 µm

Table 3 Summary of coating characteristics for Ti-6Al-4V buildup as-sprayed and subject to vacuum heat treatment

Condition	As-sprayed	Recrystallization annealed at 925 °C	β- annealed at 1025 °C
Porosity	2.71%	1.03%	0.7%
Hardness (HV_{100gf})	261 ± 27	361 ± 24	400 ± 11
Oxygen content	0.768%	0.776%	0.776%

with all particles below 20 µm (Fig. 2). The SEM micrographs in Fig. 3 show that the particles are fully dense and feature a smooth surface, facilitating powder flow. The oxygen content in the powder of 0.25% was measured with a LECO 836 Series Elemental Analyzer. Phase analysis was carried out by x-ray diffraction (XRD) using a Bruker D8-Discovery diffractometer (Bruker AXS Inc.,Madison, WI) with Cu K_α radiation at an acquisition of rate of 0.01°/s and confirms an exclusive α/α' phase composition of the starting powders, while no other phases could be detected.

The resulting spray coatings were analyzed by optical microscopy and SEM. Porosity was estimated by image analysis at 200x. Vickers hardness was measured at 100 g force (HV_{100gf}).

Selected coating samples were removed from the substrate by EDM machining and subjected to vacuum heat treatment. Recrystallization annealing was conducted at a heating rate of 10 °C/min up to 925 °C, a temperature slightly lower than the α → ß transition of 995 °C. At the same heating rate, beta-annealing was implemented up to 1025 °C, slightly above the α → ß transition temperature. The maximum temperature was maintained for 1 h, followed by oven cooling at a rate slower than 350 °C/min.

Tensile testing (MTS 810, MTS Systems Corp., Eden Prairie, USA) was performed with specimens based on small-scale testing using gage dimensions of 14 × 1 mm, which have a length-to-width ratio similar to sheet-type specimens in ASTM E8/E8M-22 (Ref 24). In-plane specimens with a tensile direction perpendicular to the traverse direction were produced by machining the tensile geometry using EDM followed by milling and cutting 1-mm-thick sections. The rate of the actuator (i.e., grip) movement was 0.21 mm/min with the specimen elongation based on the change in extensometer position at 12.5 mm. Tensile specimen sizes for freestanding Ti-6Al-4V coupons are shown in Fig. 4.

Results and Discussion

Process Parameter (TAFA 825 JP*id*)

Figure 5 shows optical micrographs of typical Ti-6Al-4V coatings produced at low (360 slpm) and high (575 slpm) nitrogen flows for varying combustion powers, as imposed by increasing amount of kerosene flow. Instead of a splat structure typically found in thermal spray coatings, the microstructures show compaction of partially deformed particles with different degrees for interface bonding, suggesting a solid-state deposition. Coating thickness was maintained at approximately 350 µm at a deposition efficiency of 80-95%. Increasing the kerosene flow induces a decrease in coating porosity, as summarized in Fig. 6(a). The evolution of the microstructures in Fig. 5 suggests closer particle packing and increased particle deformation at higher input power possibly due to a combined effect of increased particle impact velocity and particle softening. At the moderate nitrogen flows (360 slpm), the particle boundaries are well visible in the optical micrographs, possibly due to the formation of an oxide layer on the particle surfaces. The SEM micrograph inserts of the etched cross section (using Kroll reagent) at higher magnifications emphasize the preferentially etched oxide layers on the boundaries. These interfaces become slightly less apparent at higher nitrogen flow (575 slpm) (Fig. 5d and e), and the etchant attack between the particles is less severe, suggesting less oxide formation and improved bonding. Figure 6(a) further shows slightly higher hardness values (∼ 370 HV_{100gf}) for the coatings produced at higher nitrogen flows, at similar porosities than obtained at the lower flows, which may confirm improved metallurgical bonding. Preferential bonding is generally attributed to increased particle impact velocity (Ref 22). The higher nitrogen flows likely impart higher gas and particle velocities, thereby lowering the particle residence time in the flame and cool the flame to balance the particle temperatures, thereby mediating in-flight oxide scale formation.

Figure 6(b) shows the porosity and oxide content evolution with increasing standoff distance. A slight densification is observed, which may be related to an increased residence time of the particles in the flame available for particle heating and softening. At the same time, an increase in oxygen pickup in the coating from 0.62 to 0.76% is found. While differences in hardness of ∼ 345-360 HV_{300gf} in these coatings could not be found, the increase in oxygen content suggests that the particle residence time may indeed directly affect oxide scale formation and particle bonding.

Process Scale-up and Heat Treatment (TAFA 825 JPid)

Preferential spray conditions using high power at 9 lph kerosene/300 slpm oxygen in conjunction with an elevated nitrogen flow of 575 slpm to improve particle bonding

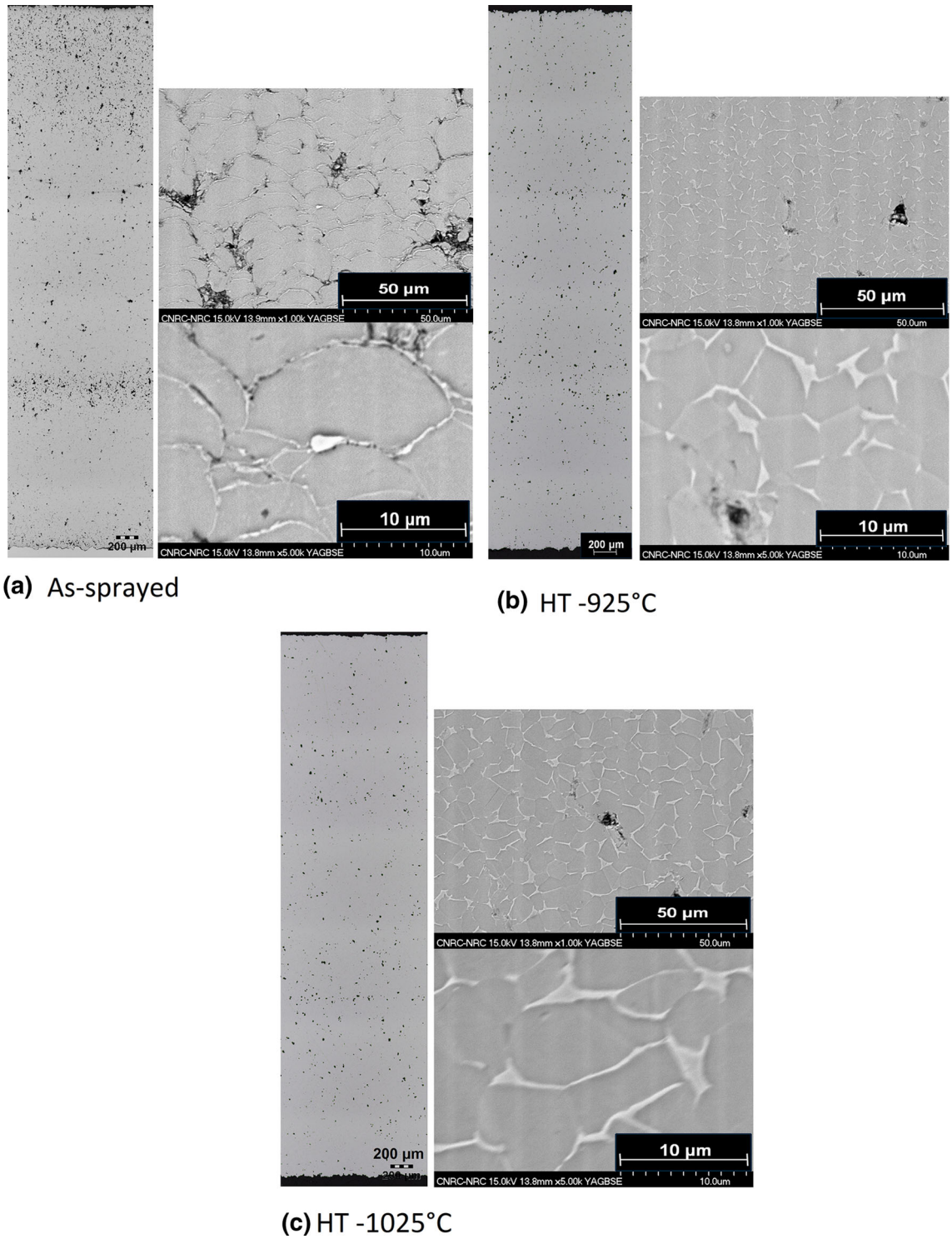

Fig. 8 Cross-sectional optical micrographs of non-etched Ti-6Al-4V over coating thickness (~ 5 mm) and representative SEM images of Kroll reagent etched cross sections. **a** As-sprayed coating and **b** coating subjected to vacuum heat treatment for recrystallization annealing at 925 °C and **c** beta-annealing at 1025 °C

were chosen to scale the thin 350 µm coatings to thicker buildups. Balancing porosity and oxygen pickup, a spray distance of 38.1 mm was used. Figure 8(a) shows micrographs of a ~ 5-mm-thick Ti-6A-4 V as-sprayed coating produced on a 114-mm-diameter steel mandrel, as depicted in Fig. 7. Cross sections of the full coating width (optical) along with representative SEM images after etching are depicted. While a thin porous layer is seen at

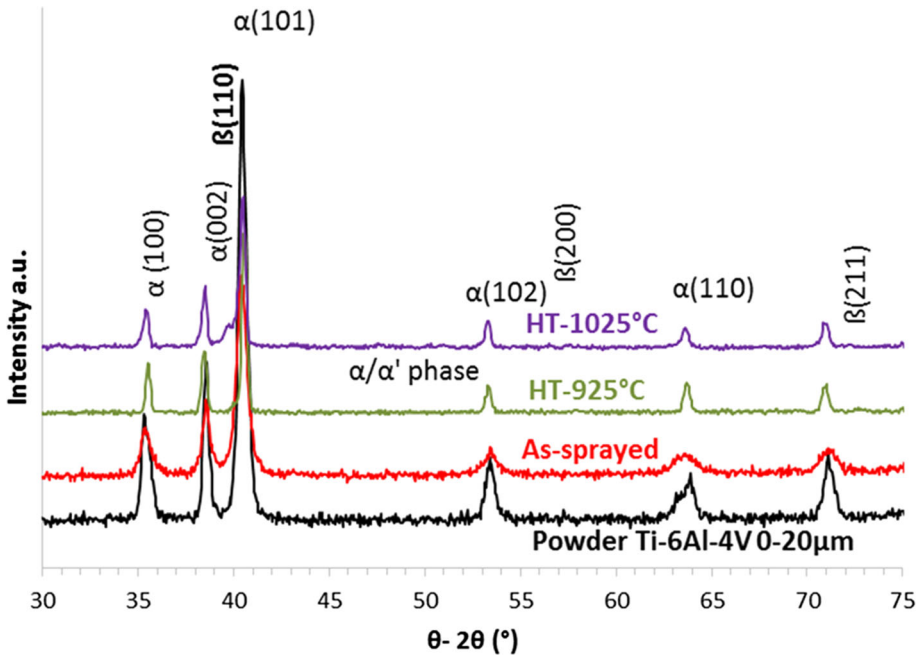

Fig. 9 XRD spectra of feedstock powder and as-sprayed and heat-treated buildup with JP*id*-825, showing the ß (110) line in the HT-1025 °C sample

approximately one mm thickness, which is attributed to a non-intended process shutdown and subsequent start-up, the bulk of the coating is rather dense with a slightly more porosity region toward the top 600 microns of the coating. In the bulk of the deposit, the etched cross section shows rather good particle contact and bonding. Table 3 summarizes the measured coating characteristics. While the values of oxygen content of 0.76% and deposition efficiency of 94.3% are expected from the previous tests, it is interesting to note that the as-sprayed porosity of 2.7% and hardness of 261 ± 27 HV100gf are somewhat lower than in the thinner coatings described earlier. The densification for the thicker coating with respect to the thinner coupons may be caused by an extended compacting effect of the impacting particle on the underlying coating during the longer coating process, as commonly seen in cold spraying. The slightly higher porosity in the top region of the coating, visible in the optical image in Fig. 8(a), may also suggest that the underlying layers are more compacted than the top layers, driving down the overall porosity in thicker solid-state buildups. A sintering effect due to the extended exposure of the coating to 120-150 °C for the duration of the deposition may also be possible.

To investigate the potential of such coating for near-net shape forming, the Ti-6Al-4V buildup was removed from the underlying substrate and subjected to vacuum heat treatment for recrystallization and beta-annealing. Figure 8 summarizes the microstructural evolution of the coatings as a function of annealing temperature. Porosity, hardness and oxygen content are given in Table 3. Both annealing temperatures induced a significant densification of the coatings down to 0.7% porosity. Zones of porosity in the as-sprayed coating such as in the top layers and a mid-layer (caused by a spray process upset) are fully homogenized and distributed uniformly throughout the coating. Further, the original particle boundaries became largely fused, resulting in an increase in hardness. The material appears fully reconstructed and transformed into equiaxial α grains with intergranular ß, which is expected to impart beneficial mechanical properties. Similar densification of cold-sprayed Ti6Al4V deposits was observed by Bhowmik et al., reporting metallurgical bonding and the disappearance of all spat interfaces at vacuum heat treatment temperature of 950 °C (Ref 19). In particular, a high ß-phase content contributes to formability of the alloy, which may result in higher elongation to failure in tensile testing, as discussed in a later section. For the heat-treated samples, the lighter phase in the SEM micrographs represents the ß phase component. The presence of the ß phase in the beta-annealed sample was confirmed by XRD though a small diffraction signal at the ß (110) line, as shown in Fig. 9. It is interesting to note the α-grain grown at 1025 °C (beta-annealing) over the 925° recrystallization. No interlamellar α could be discerned, possibly because of the high oxygen content in the coating stabilizing the α-phase.

Process Parameters (ID-Nova MK6)

Figure 10 shows optical micrographs (500x) of approximately 400-µm-thick Ti-6Al-4V coatings produced with the ID-Nova MK-6 system at increasing torch power from

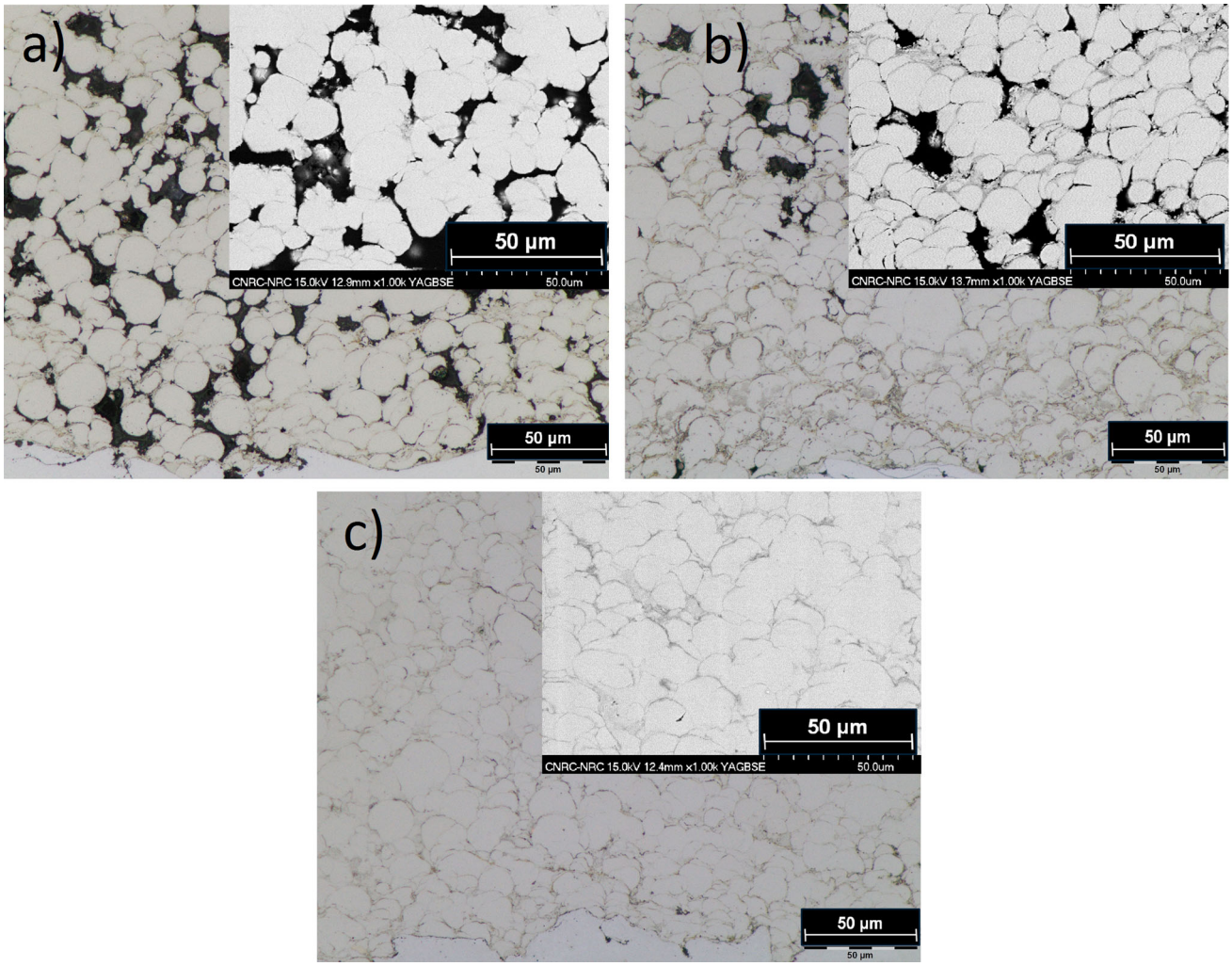

Fig. 10 Cross-sectional optical images (500 ×) of Ti-6Al-4V coatings fabricated at 40 mm standoff distance at **a** 250 H_2/125 O_2/250 N_2 **b** 270 H_2/135 O_2/250 N_2 **c** 290 H_2/145 O_2/250 N_2 (Inserts: SEM micrographs of non-etched cross section at 1000 × original magnification, showing different degrees of gray oxide layers around the particles)

Table 4 Summary of coating characteristics for Ti-6Al-4V with increasing ID-Nova MK-6 torch power

Net power and gas flow (slpm) conditions	45 kW net power 250 H_2/125 O_2/250 N_2	49 kW net power 270 H_2/135 O_2/250 N_2	52 kW net power 290 H_2/145 O_2/250 N_2
Deposition efficiency	~ 70%	~ 90%	~ 98%
Porosity	15%	8%	0.2%
Hardness	< 150 HV_{100gf}	314 ± 39 HV_{100gf}	210 ± 20 HV_{100gf}
Oxygen content	1.94%	1.74%	1.06%

45 to 52 KW through varying the hydrogen and oxygen flowrates, while maintaining a high inert gas flow (N_2) of 250 slpm and a standoff distance of 40 mm. Similar to the previous system, the coatings are formed by consolidation and ductile deformation of particles in a solid-state process. Increasing the input power drastically reduces the porosity from 16% in (a) to 8% in (b) down to 0.2% in (c) at the highest power and drives the deposition efficiency from ~ 70% to close to 100%, as summarized in Table 4. It is interesting to note that at the lower powers, the particles are barely deformed and exhibit a significant oxide scale, as indicated by the gray particle boundaries visible in the micrographs even without etching. These oxide scales possibly further impeding particle bonding and contribute

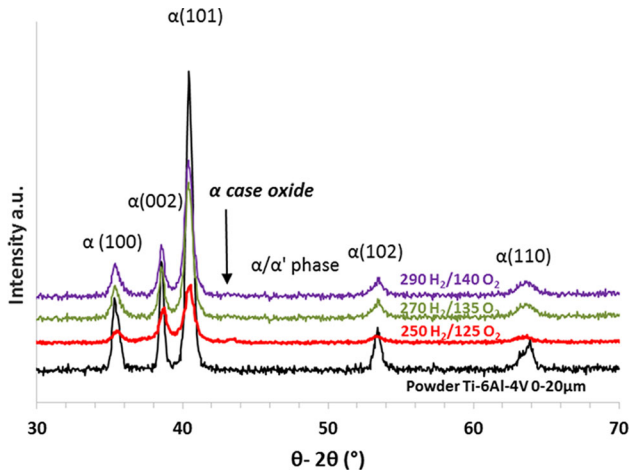

Fig. 11 XRD spectra of feedstock powder and coatings produced at increasing torch power with the ID-Nova MK-6, showing a small diffraction peak at 42.5° θ-2θ indicative of the α-case (oxide scale) at the lower torch powers

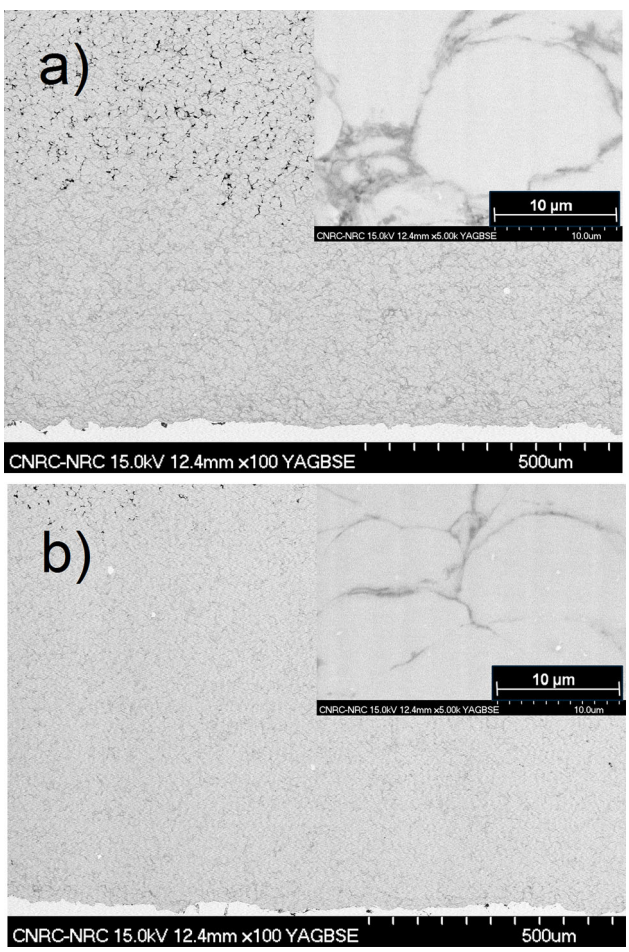

Fig. 12 Cross-sectional SEM images (100 ×) of 2-mm-thick Ti-6Al-4V coatings produced at **a** 270 H_2/135 O_2/ 250 N_2 **b** 290 H_2/145 O_2/ 250 N_2 (inserts: SEM micrographs of non-etched cross section at 5000 × original magnification, showing different degrees of gray oxide layers at the particle interfaces)

to the high porosity. The denser regions in (b) appear to be formed by oxides and small fines filling the gaps. The oxide content in coating (b) is 1.74 ± 0.07% with a coating hardness of 300 ± 61 HV_{100gf}. In contrast, the coating produced at the highest power (c) shows a lower oxide content of 1.06 ± 0.1% and a lower hardness of 210 ± 20 HV_{100gf}, suggesting a superior degree of particle bonding with less oxide scale. The XRD spectra in Fig. 11 suggest the presence of α-case (oxide scale) at the lower-power conditions. It is possible that at the highest gas flow rates, although at higher power, the higher particle velocity and lower residence time limit in-flight oxidation of the particles and create the superior coating. Since the higher power condition is associated with the higher gas flow rates, it is possible that the resulting higher particle velocity and shorter residence time limit the in-flight oxidation and create a superior coating.

Process Scale-up and Heat Treatment (ID-Nova MK6)

The preferential spray conditions at the higher net powers were scaled to a coating thickness of ∼ 2 mm. Figure 12 shows the SEM microstructures of the as-sprayed coatings at 49 and 52 kW net power. Deposition efficiencies, oxygen content and hardness was preserved by the scaling. However, for the 49 kW condition the overall porosity is reduced from ∼ 8% (Fig. 10b) to below 3.5% (Fig. 12a) and the residual porosity is primarily found in the top layers of the coating. This feature was consistent for all coatings produced with the ID-Nova MK6 and maybe an indication that there is a compaction effect on the underlying layers by the impinging solid-state particles, similar to the observations made for the JP*id* 825 coatings above.

These thicker coatings were subsequently removed from the underlying substrate and subjected to vacuum heat treatment for beta-annealing at 1025 °C. Optical and SEM micrographs in Fig. 13 show that the heat treatment fully fused and reconstructed the original particle boundaries, leading to increase in hardness, and ultimately transforming the material into equiaxial α grains with intergranular ß. Material characteristics of the as-sprayed and heat-treated samples are summarized in Table 5. The porosity gradients of coating a), as produced at lower power, fully disappear. Any residual porosity is homogenously disturbed throughout the layer. It is interesting to note that the remaining porosity after heat treatment does not correlate with the as-sprayed porosity and that the coating produced at higher power exhibits significantly more β-phase than the lower-power coating in Fig. 13. This is attributed to its lower oxygen content of approximately 1%, stabilizing the α-phase to a lesser extent and thereby allowing more β-phase formation. The small

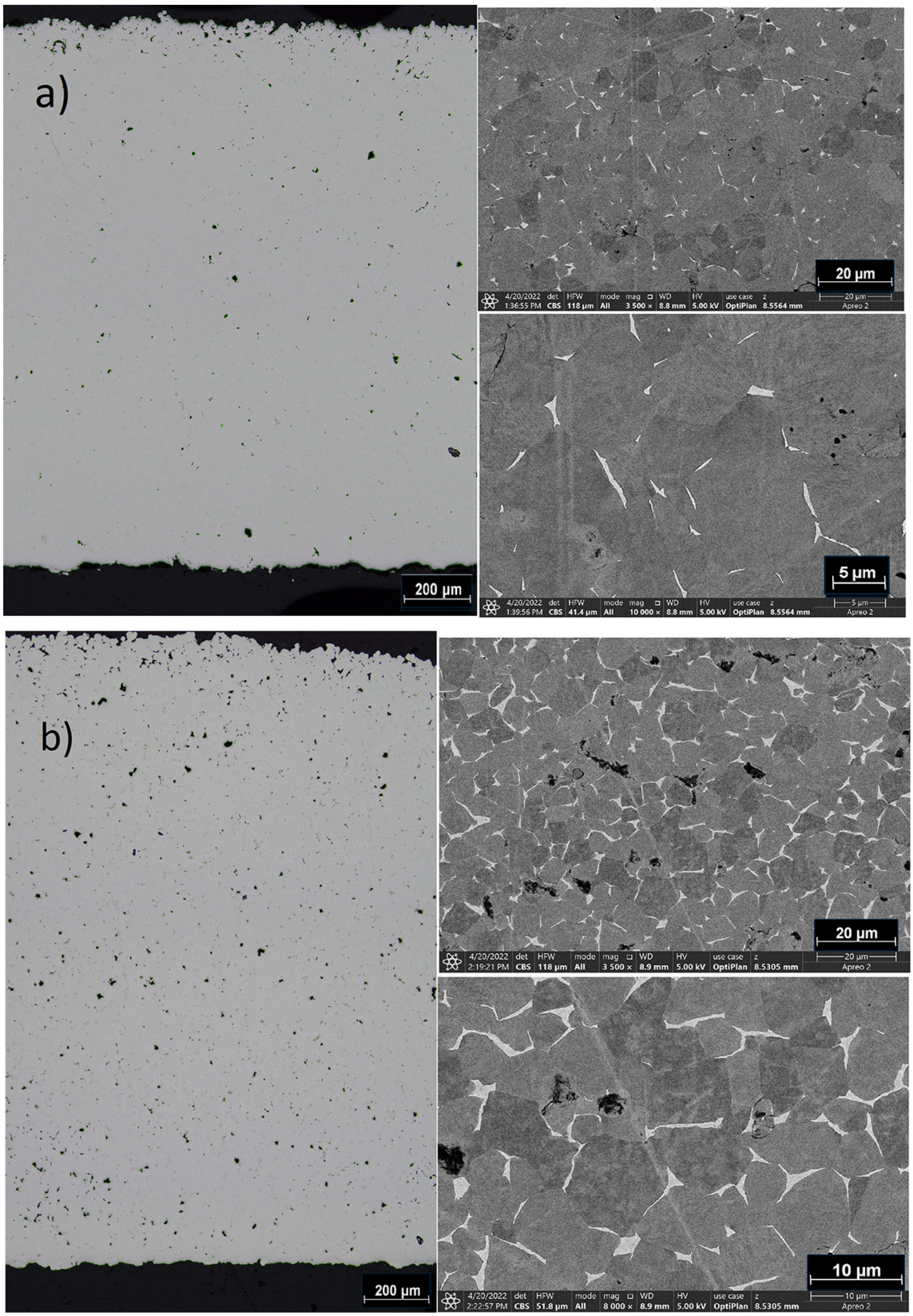

Fig. 13 Cross-sectional optical micrographs (100 ×) of thick Ti-6Al-4V produced at **a** 270 H_2/135 O_2/250 N_2 **b** 290 H_2/145 O_2/250 N_2) after beta-annealing at 1025 °C and representative SEM images (3.5 kx and 10kx) showing equiaxial α grains (dark gray phase) with intergranular ß phase (light phase)

Table 5 Summary of coating characteristics for ~ 2-mm-thick Ti-6Al-4V ID-Nova MK-6 coatings before and after heat treatment

Spray condition	49 kW 270 H_2/135 O_2/ 250 N_2		52 kW 290 H_2/145 O_2/ 250 N_2	
Heat treatment	As-sprayed	β- annealed at 1025 °C	As-sprayed	β-annealed at 1025 °C
Porosity	3.4%	0.53%	0.2%	0.82%
Hardness	315 ± 25 HV_{100gf}	490 ± 31 HV_{100gf}	210 ± 20 HV_{100gf}	390 ± 15 HV_{100gf}
Oxygen content	1.74%	1.75%	1.02%	1.05%

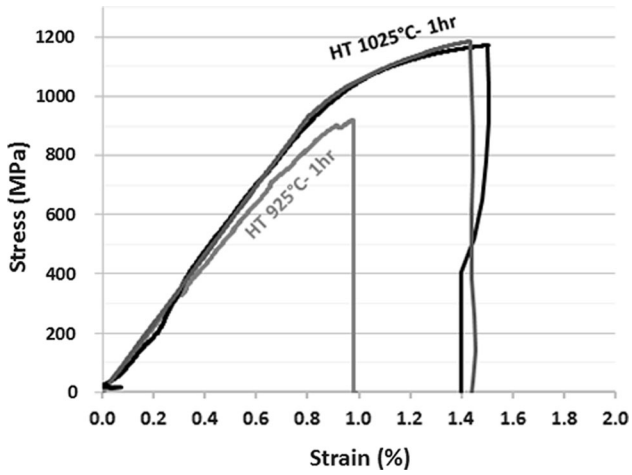

Fig. 14 Representative stress–strain curves for HVOF coupons subjected to recrystallization (925 °C) and β-annealing (1025 °C)

Table 6 Tensile strength and elongation to failure values for as-sprayed and annealed coatings (five replicates per sample)

Anneal temp, °C	Anneal. time, h	Hardness, HV_{100gf}	UTS, MPa	El, %
As-sprayed	…	261 ± 27	< 150	0
925 °C	1 h	361 ± 24	889 ± 49	1.0 ± 0.3
1025 °C	1 h	400 ± 11	1126 ± 61	1.3 ± 0.2

increase in porosity from 0.2 to 0.8% during β-annealing is likely caused by shrinkage due to phase transformation, while the original pores are likely fully fused.

Tensile Testing and Mechanical Properties

The mechanical properties of selected coatings were evaluated by tensile testing following the ASTM standard E8/E8M-22 (Ref 24). For these test, freestanding and heat-treated sections of the coating were machined into tensile test coupons, as described above. Due to an oxygen content of 1% and above in multiple samples, only the samples with the lowest oxygen content, as produced by the JP*id*-825 system, are considered at this stage of the study. An average of five specimen per conditions were recorded. Figure 14 shows representative stress–strain curves for recrystallization and β-annealed coupons. Two replicates are shown for the β-annealed coupons. Table 6 summarizes the mechanical properties of the HVOF-sprayed Ti-6Al-4V buildups.

The attained ultimate tensile strength of ~ 890 MPa after recrystallization and in particular 1126 MPa after beta-annealing compares highly favorable to the values reported in the literature, which are generally below 900 MPa for coatings produced by low- and high-pressure HVOF warm spraying, cold spraying, low-pressure plasma spraying or bulk material. However, the elongation at failure of ~ 1% is low in comparison with the literature data. The formability of Ti-6Al-4V and, by consequence, its elongation at failure is related to both the microstructure of the material and the amount of β-phase. The limited elongation here is likely due to high level of α-phase stabilization, thereby suppressing the β-phase, by the residual oxygen content in the buildup of approximately 0.7%. Further reduction in this oxygen content both from the feedstock and processing side would be required to further improve these properties.

Conclusion

This study illustrates the potential viability of using novel miniaturized HVOF systems for the production of near-net-shaped Ti-6Al-4V materials. In particular, the addition of nitrogen into the combustion was implemented in these smaller systems to improve as-sprayed coating porosity by increasing the gas and particle velocity and mediate the particle heating to limit oxide scale formation. Both the kerosene- and hydrogen-fuelled systems demonstrated very high deposition efficiencies above 80% for coatings or parts reaching multiple millimeters in thickness. As-spayed coatings can attain porosities well below 3%. Post-treatment through recrystallization and beta-annealing fuses the as-sprayed coating structure into nearly fully dense buildups and transforms the material into equiaxial α grains with intergranular ß. The amount of beta phase increases with both increasing annealing temperature and decreasing oxygen content. For these HVOF buildups, beta-annealing can generate exceptional ultimate tensile strength with UTS over 1100 MPa. To further improve the mechanical

properties, a key challenge is the reduction in the residual oxygen content in the coating to improve particle bonding and to avoid α-phase stabilization, thereby allowing for β-phase creation for higher elongation at failure and formability.

Funding Open Access provided by National Research Council Canada.

References

1. G. Lutjering and J.C. Williams, *Titanium*, 2nd ed. Springer, Berlin, 2003.
2. R.H. Morgan, C.J. Sutcliffe, J. Pattison, M. Murphy, C. Gallagher, A. Papworth, P. Fox, and W. O'Neill, Cold Gas Dynamic Manufacturing—A New Approach to Near-Net Shape Metal Component Fabrication, *Mater. Res. Soc. Symp. Proc.*, 2003, **758**, p 73-84.
3. E. Brandl, A. Schoberth, and C. Leyens, Morphology, Microstructure, and Hardness of Titanium (Ti-6Al-4V) Blocks Deposited by Wire-Feed Additive Layer Manufacturing (ALM), *Mater. Sci. Eng. A*, 2012, **532**, p 295-307.
4. J. Cizek, O. Kovarik, J. Siegl, K.A. Khor, and I. Dlouhy, Influence of Plasma and Cold Spray deposited Ti Layers on High-Cycle Fatigue Properties of Ti6Al4V Substrates, *Surf. Coat. Technol.*, 2013, **217**, p 23–33.
5. L.E. Murr, S.A. Quinones, S.M. Gaytan, M.I. Lopez, A. Rodela, E.Y. Martinez, D.H. Hernandez, E. Martinez, F. Medina, and R.B. Wicker, Microstructure and Mechanical Behavior of Ti-6Al-4V Produced by Rapid-Layer Manufacturing, for Biomedical Applications, *J. Mech. Behav. Biomed. Mater.*, 2009, **2**(1), p 20-32.
6. H.R. Salimijazi, T.W. Coyle, and J. Mostaghimi, Vacuum Plasma Spraying: A New Concept for Manufacturing Ti-6Al-4V Structures, *JOM-US*, 2006, **58**, p 50-56.
7. R.E. Blose, B.H. Walker, R.M. Walker, and S.H. Froes, New Opportunities to Use Cold Spray Process for Applying Additive Features to Titanium Alloys, *Met. Powder Rep.*, 2006, **61**, p 30-37.
8. J.C. Lee, H.J. Kang, W.S. Chu, and S.H. Ahn, Repair of Damaged Mold Surface by Cold-Spray Method, *Ann. CIRP*, 2007, **56**, p 577-580.
9. V.K. Champagne, The Repair of Magnesium Rotorcraft Components by Cold Spray, *J. Fail. Anal. Prev.*, 2008, **8**, p 164-175.
10. R. Huang and H. Fukanuma, Study of the Influence of Particle Velocity on Adhesive Strength of Cold Spray Deposits, *J. Therm. Spray Technol.*, 2012, **21**(3-4), p 541-549.
11. W. Wong, E. Irissou, J.G. Legoux, P. Vo, and S. Yue, Powder Processing and Coating Heat Treatment on Cold Sprayed Ti-6Al-4V Alloy, *Mater. Sci. Forum.*, 2012, **706-709**, p 258-263.
12. P. Vo, E. Irissou, J.-G. Legoux, and S. Yue, Mechanical and Microstructural Characterization of Cold-Sprayed Ti-6Al-4V After Heat Treatment, *J. Therm. Spray Technol.*, 2013, **22**(6), p 954-964.
13. D.L. Gilmore, R.C. Dykhuizen, R.A. Neiser, T.J. Roemer, and M.F. Smith, Particle Velocity and Deposition Efficiency in the Cold Spray Process, *J. Therm. Spray Technol.*, 1999, **8**(4), p 576-582.
14. J. Kawakita, H. Katanoda, M. Watanabe, K. Yokoyama, and S. Kuroda, Warm Spraying: An Improved Spray Process to Deposit Novel Coatings, *Surf. Coat. Technol.*, 2008, **202**(18), p 4369-4373.
15. S. Kuroda, M. Watanabe, K.-H. Kim, and H. Katanoda, Current Status and Future Prospects of Warm Spray Technology, *J. Therm. Spray Technol.*, 2011, **20**(4), p 653-676.
16. S. Kuroda, J. Kawakita, M. Watanabe, and H. Katanoda, Warm Spraying—A Novel Coating Process Based on High-Velocity Impact of Solid Particles, *Sci. Technol. Adv. Mater.*, 2008, **9**(3), p 1-17.
17. R.M. Molak, H. Araki, M. Watanabe, H. Katanoda, N. Ohno, and S. Kuroda, Effects of Spray Parameters and Post-spray Heat Treatment on Microstructure and Mechanical Properties of Warm-Sprayed Ti-6Al-4V Coatings, *J. Therm. Spray Technol.*, 2017, **26**, p 627-647.
18. D. MacDonald, R. Fernandez, F. Delloro, and B. Jodoin, Cold Spraying of Armstrong Process Titanium Powder for Additive Manufacturing, *J. Therm. Spray Technol.*, 2017, **26**(4), p 598-609.
19. A. Bhowmik, A.W.Y. Tan, W. Sun, Z. Wei, I. Marinescu, and E. Liu, On the Heat-Treatment Induced Evolution of Residual Stress and Remarkable Enhancement of Adhesion Strength of Cold Sprayed Ti–6Al–4V Coatings, *Results Mater.*, 2020, **7**, p 100119. https://doi.org/10.1016/j.rinma.2020.100119
20. V.S. Bhattiprolu, K.W. Johnson, and G.A. Crawford, Influence of Powder Microstructure on the Microstructural Evolution of As-Sprayed and Heat Treated Cold-Sprayed Ti-6Al-4V Coatings, *J. Therm. Spray Technol.*, 2019, **28**, p 174-188. https://doi.org/10.1007/s11666-018-0812-1
21. V.N.V. Munagal, V. Akinyi, P. Vo, and R.R. Chromik, Influence of Powder Morphology and microstructure on the Cold Spray and Mechanical Properties of Ti6Al4V Coatings, *J. Therm. Spray Technol.*, 2018, **27**, p 827-842.
22. R.M. Molak, H. Araki, M. Watanabe, H. Katanoda, N. Ohno, and S. Kuroda, Warm Spray Forming of Ti-6Al-4V, *J. Therm. Spray Technol.*, 2014, **23**(1-2), p 197-212.
23. P. Khamsepour, J. Oberste-Berghaus, M. Aghasibeig, F. Ben Ettouil, C. Moreau, and A. Dolatabadi, The Effect of Spraying Parameters of the Inner-Diameter High-Velocity Air-Fuel (ID-HVAF) Torch on Characteristics of Ti-6Al-4V In-Flight Particles and Coatings Formed at Short Spraying Distances, *J. Therm. Spray Technol.*, 2022, **18**, p 164.
24. Standard Test Methods for Tension Testing of Metallic Materials, *ASTM E8/E8M-22*, ASTM International, West Conshohocken, 2022.